A NEGATIVE DIELECTROPHORESIS BASED METHOD OF DETECTING PANCREATIC CANCER ANTIGEN CA 242 IN SERUM

A Thesis
Submitted to the Graduate Faculty
of the
North Dakota State University
of Agriculture and Applied Science

By

Sharmin Afrose

In Partial Fulfillment of the Requirements
for the Degree of
MASTER OF SCIENCE

Major Department:
Electrical and Computer Engineering

July 2020

Fargo, North Dakota

North Dakota State University
Graduate School

Title

A NEGATIVE DIELECTROPHORESIS BASED METHOD OF DETECTING PANCREATIC CANCER ANTIGEN CA242 IN SERUM

By

Sharmin Afrose

The Supervisory Committee certifies that this ***disquisition*** complies with North Dakota State University's regulations and meets the accepted standards for the degree of

MASTER OF SCIENCE

SUPERVISORY COMMITTEE:

Dr. Ivan T. Lima Jr.
Chair

Dr. Dali Sun

Dr. Mohiuddin Quadir

Approved:

07/09/2020
Date

Benjamin Braaten
Department Chair

ABSTRACT

Patients with pancreatic cancer in metastasis rarely survive, thus the need for diagnostic tools for early stage detection. Current techniques such as ELISA and SPR are complex and expensive and cannot detect cancer in its early stages. Cancer Antigen 242 (CA 242) is a potential protein biomarker of pancreatic cancer with high sensitivity and specificity. This thesis presents a negative Dielectrophoresis (DEP) based method of detecting pancreatic cancer protein biomarker CA 242 in serum. A spectrum of concentration levels was generated with a cut off level 20 U/mL using a transduction mechanism with negative DEP spectroscopy, light scattering, and image processing. This was a fast and cost-effective method to diagnose early stage pancreatic cancer. This thesis also presents the design and simulation of an electrode modified to increase the electric field gradient with reduced heat generation and a concentration prediction model to predict concentrations from the generated spectrum of experiments.

ACKNOWLEDGEMENTS

I would like to thank my parents and my siblings for their continuous and unconditional love and support, without which I wouldn't be what I am today. I would like to specially thank my mother for always encouraging me through difficult times and giving all the opportunities that I could asked for. I want to express my gratitude to my advisor, Dr. Ivan T. Lima Jr. for providing all the guidance and support that I needed in every step of the way to complete this thesis, I have learned so much from him that would stay with me in the next endeavor of my career. I am thankful to Dr. Dali Sun and Dr. Mohiuddin Quadir for serving in my thesis committee. I would also like to thank my colleagues, Fleming Gudagunti, Logeeshan Velmanickam, Julian Thrash, and Vidura Jayasooriya for their help and support throughout my thesis work. I am thankful to my husband Md Ashiqur Rahaman Khan for providing me unconditional support in completing my graduation. I also must mention the continuous love and mental support I received from my friends, Masuma Rumi and Mitu Roy during my master program. Last but not the least, I would like to thank my roommates, Tajnin Sultana and Samara Choudhury for their kindhearted support and giving me the feeling of my home in me abroad like that made the last year of my life a very memorable experience.

DEDICATION

To my parents, siblings, and my husband for their kind prayers, love and support.

TABLE OF CONTENTS

LIST OF TABLES

LIST OF FIGURES

LIST OF ABBREVIATIONS

AC .....Alternating Current

BSA.....Bovine Albumin Serum

CA .....Cancer Antigen

CEA.....Carcinoembryonic Antigen

CI.....Confidence Interval

DC .....Direct Current

DEP .....Dielectrophoresis

DNA .....Deoxyribonucleic Acid

EC .....Electric Current

ELISA .....Enzyme Linked Immunosorbent Assay

EM.....Electromagnetic

FDA.....Food and Drug Administration

PBS .....Phosphate Buffet Saline

PM.....Polystyrene Microspheres

POC.....Point of care

RNA .....Ribonucleic Acid

SD .....Standard Deviation

SERS .....Surface enhanced Raman scattering

SPR .....Surface Plasmon Resonance

UVC .....USB video class

1. INTRODUCTION

Cancer, a life-threatening disease, has a very low survival rate. Pancreatic cancer is one of the deadliest cancers in the world and is characterized by its rapid malignance. Therefore, diagnosis of this cancer at a very early stage can significantly reduce the death rate [1]. Currently, research and development of several diagnosis methods for early stage pancreatic cancer is ongoing. Biosensors are a promising tool for early pancreatic cancer detection because of their ease of use, low cost, and quick results [2, 3].

1.1. Pancreatic Cancer

Pancreatic cancer is a ductal adenocarcinoma of the pancreas [4, 5]. According to the American Cancer Society, by 2020 about 57,600 people will be diagnosed with pancreatic cancer and about 47,050 people will die of pancreatic cancer. Pancreatic cancer accounts for about 3% of all cancers in the US and about 7% of all cancer deaths. Survival rates can give an idea of what percentage of people with the same type and stage of cancer are still alive 5 years after they were diagnosed. The 5-year survival rate of pancreatic cancer is currently only 9% in the US [6]. One of the reasons is that the cancer is not diagnosed in its early stage, but after it has already spread to other organs. Though the actual cause of pancreatic cancer is unknown, data suggest that gene mutations are responsible [7].

Methods for diagnosing pancreatic cancer are complex, costly, and unable to detect cancer in its early stages. Medical imaging systems are popular in pancreatic cancer diagnosis when cancer has already spread and the patient has significant symptoms [8, 9]. Some patients require additional diagnosis such as endoscopic ultrasonography when significant masses are not visible in medical imaging. Some methods require tissue samples through biopsy, which is a complex and painful procedure. The recent development of protein biomarker detection eases the

process of pancreatic cancer detection at a very early stage. There are several potential protein serum biomarkers available for the diagnosis and prognosis of pancreatic cancer such as CA 19-9, CA 242, CEA etc. Cancer Antigen (CA) 19-9 is an FDA approved biomarker [10, 11], but it has some limitations of low sensitivity and specificity. The level of CA 19-9 may be elevated in other adverse conditions of health such as cholestasis. Therefore, using a panel of biomarkers would increase the sensitivity and specificity for pancreatic cancer detection [12].

1.2. Cancer Antigen (CA) 242

Cancer Antigen (CA) 242 is a complementary protein biomarker of pancreatic cancer, which has higher sensitivity and specificity than other biomarkers of this cancer [13, 14, 15]. It is a mucoprotein type of carbohydrate antigen that is acidic in saliva and rarely found in normal tissues. Patients with pancreatic cancer have more than 20 U/mL of CA 242 in blood serum, whereas patients with CA 242 lower than 20 U/mL in blood serum are considered as the control group without cancer. The sensitivity and specificity of CA 242 is 75% and 85%, respectively [14, 15]. A comparison table of the biomarkers is presented in table 1.

Table 1. Meta-analysis of CA19-9, CA242, and CEA for detecting pancreatic cancer [16].

Pooled estimates	CA19-9	CA242	CEA
Sensitivity (%) (95% CI)	75.4	67.8	39.7
Specificity (%) (95% CI)	77.6	83	81.3

The biomarkers can be detected simultaneously with multiplexing as their combined sensitivity and specificity is higher than individual marker. The combined biomarker comparison is summarized in table 2.

Table 2. Sensitivity and specificity of combination test [16].

Biomarkers	Sensitivity (%)	Specificity (%)
Parallel Combination		
CA19-9+CA242	89	75
CA19-9+CEA	85	71
CA242+CEA	76	71
CA19-9+CA242+CEA	90	64
Serial combination		
CA19-9+CA242	66	87
CA19-9+CEA	52	80
CA242+CEA	58	89
CA19-9+CA242+CEA	50	93

1.3. Biosensors for Protein Biomarker Detection

Biosensors are analytical devices that detect a biological target analyte by converting a biorecognition event with transducer into a sensing or signal processing unit for analysis. For example, the biological targets can be antibodies, antigens, enzymes, peptides, aptamers, DNA, microorganisms, and ligands, and the transduces can be electrochemical, optical, calorimetric, magnetic or based upon mass changes (figure 1). The transducer converts any biological event, such as antibody-antigen, DNA-DNA, and DNA-RNA, to a measurable signal that occurs due to the physical or chemical change depending on the concentration of biological analytes [17]. Many biosensors are now commercially available as they have certain advantages such as sensitivity, specificity, low cost, and fast analysis. Biosensors are now used extensively for cancer diagnosis due to biomarker discovery, easy detection, and analysis techniques [17, 18].

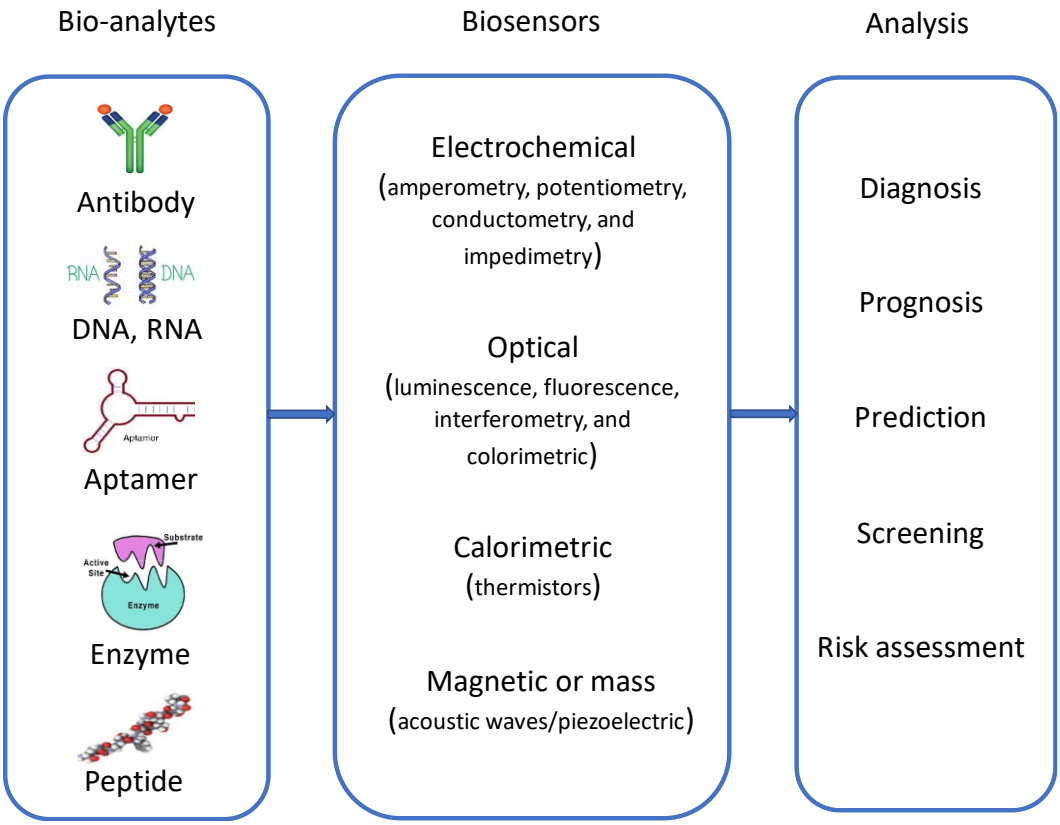

Figure 1. Biosensor working process.

The advent of various cancer biomarkers, such as proteins, nucleic acids, cancer cells, and exosomes in blood or serum of cancer patient, made the early detection of cancer more convenient. The potential biomarkers are those which have high sensitivity and specificity. The potential biomarkers for pancreatic cancer are CA 19-9, CA 242, CEA etc.

The commonly used methods are currently immunosensors such as Enzyme Linked Immunosorbent Assay (ELISA) that uses antibody-antigen interaction, and Surface Plasmon Resonance (SPR) that uses optical sensing [19, 20]. ELISA uses the microtiter plates that contains the capture antibody, and the cancer antigen from the serum is placed in the solution and incubated. The capture antibodies are usually tagged with fluorescent dyes or other reagents. Albeit having flexibility and easiness of use, using of this require expertise and time and hardly use for Point of Care (POC) applications [21]. Optical biosensors use the change in wavelength

to transform the biological event into electrical signal using optical transducers. SPR and surface enhanced Raman scattering (SERS) are popular among them [19, 20]. They use label-free probing and generate surface charge wave when EM wave propagates in dielectric particle and thin metal layer [18].

For POC application, the methods with short time and portability are crucial. Electrochemical biosensors use electrochemical transducer to convert biological phenomenon into an electrical signal and is used today for their cost effectiveness, feasible miniaturization, ease of use, and portability. These sensors use the techniques amperometry, potentiometry, impedance spectroscopy, capacitance measurement, and dielectrophoresis (DEP). A label-free DEP based method was developed to detect CA 19-9 with a concentration lower than its cut-off level 37 U/mL [27]. For higher sensitivity and specificity, CA 242 detection in serum was produced using the same DEP technique [22].

2. DIELECTROPHORESIS (DEP) BIOSENSOR

2.1. Dielectrophoresis Theory

The term Dielectrophoresis (DEP), originates from the Greek word ‘Phorein’, which was first proposed by Pohl [23]. Phorein is an effect on particles that are carried by force contingent upon their dielectric properties. Pohl defined this effect as “the motion of suspensoid particles relative to that of the solvent resulting from polarization forces produced by an inhomogeneous electric field” [24]. The effect was in fact known to the ancient Greeks and Romans. Pohl then started his struggle to develop theories and methods for the dielectrophoretic characterization and separation of biological cells and bacteria, but it took time to get the term ‘Dielectrophoresis’ well-established [24].

The behavior of a dielectric particle depends on the surrounding electric field that is uniform or nonuniform. When a dielectric particle is placed in a uniform electric field, the induced distribution of positive and negative charges experiences coulombic force with similar magnitudes but in opposite directions. So, the net electric force acting on this particle will be zero. Furthermore, Placing the charge with an angle between the moment of charge and the uniform electric field, will not produce translational force but an electrical force that causes the rotation of the particle. This rotation is due to radial force, which acts on the positive and negative charge and this force is the product of the charge and the field component along the radial direction. The net radial force induced in positive and negative charge, acting along the axis of the moment, cancel out each other. Albeit exhibiting electrophoretic mobility in a uniform electric field, which depends on the net surface charge associated with ionized chemical groups on the membrane, it does not depend on the dipole moment of the particle (See figure 2). However, when a dielectric polarized particle is placed in a nonuniform electric field, it

experiences translational forces induced in positive and negative elements of dipole moment, and the algebraic sum of the forces is not zero (See figure 3). This resultant translational force is known as *dielectrophoretic* force. This force is potentially applied in the biotechnology field to target different particles such as DNA, RNA, protein, cells, etc. that are isolated, concentrated, quantified or purified from a complex mixture. The translational force from nonuniform electric field induced in these particles creates either attraction or repulsion of the particles to or from the electrodes.

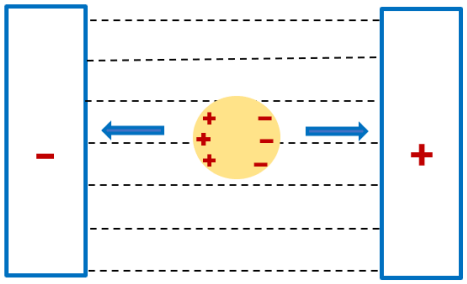

Figure 2. Uniform electric field.

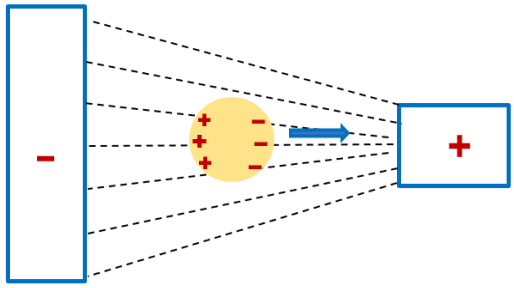

Figure 3. Non-uniform electric field.

Different lengths and shapes of electrodes can produce a nonuniform electric field with a desired electric field gradient. Such as in figure 4, a high electric field region is created on the right electrode and a low electric field region is created on the left electrode. If the particle is more polarizable than the surrounding medium, then it experiences a net force towards the high electric field region and will be attracted towards the right electrode. This phenomenon is known

as positive DEP. On the other hand, if the particle is less polarizable than the surrounding medium, then it moves toward the low electric field region on the left electrode. This process is known as negative DEP.

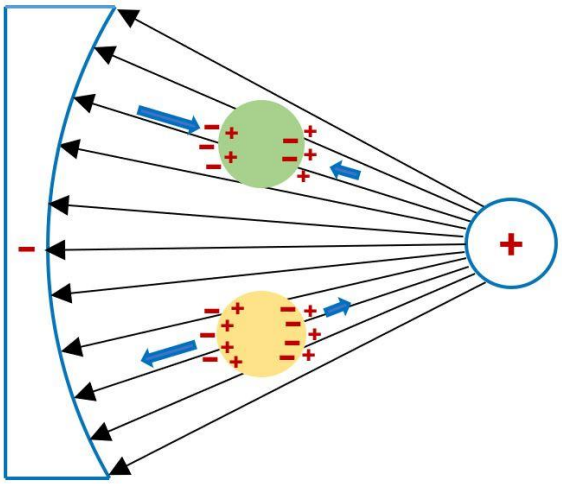

Figure 4. DEP effect on dielectric particle in non-uniform electric field.

For a spherical particle of radius r, the force of time-averaged DEP can be calculated using the following equation: [25, 26, 27]

$$\langle F_{DEP} \rangle = 2\pi\varepsilon_0\varepsilon_m r^3 Re[K_{CM}(\omega)]\nabla(E^2) \quad (1)$$

where ε_0 is the permittivity of the free space, ε_m is the relative permittivity of the medium, ∇E is the electric field gradient, and $Re[K_{CM}(\omega)]$ is the real part of the Clausius–Mossotti factor that is the effective polarizability per unit volume of the particle. It can be written as: [26, 28]

$$K_{CM} \equiv \frac{\varepsilon_p{}^* - \varepsilon_m{}^*}{\varepsilon_p{}^* + 2\varepsilon_m{}^*} \quad (2)$$

where ε_p and ε_m are the complex permittivity of the particle and the medium, respectively. The complex permittivity is expressed by the conductivity σ and the angular frequency ω of the applied alternating current (AC) field with the following equation: [29, 30]

$$\varepsilon^* \equiv \varepsilon - j\frac{\sigma}{\omega} \tag{3}$$

Then the Clausius–Mossotti factor can be written as:

$$K_{CM} \equiv \frac{\varepsilon_p - \varepsilon_m + j(\frac{\sigma_m - \sigma_p}{\omega})}{\varepsilon_p + 2\varepsilon_m - j(\frac{\sigma_p + 2\sigma_m}{\omega})} \tag{4}$$

The Clausius–Mossotti factor, $K_{CM}(\omega)$, varies from $-\frac{1}{2}$ to 1 depending on the relative values of the conductivity and angular frequency of the particle and the surrounding medium. According to the sign of $K_{CM}(\omega)$, the force is defined as positive DEP, negative DEP, and zero-force DEP. If $K_{CM}(\omega)$ is positive, then particles are attracted to the regions of high electric field intensity, an effect termed positive DEP, and if $K_{CM}(\omega)$ is negative, then the particles are repelled from the regions of high electric field intensity, an effect termed negative DEP. Since $K_{CM}(\omega)$ is frequency dependent, both positive and negative DEP effects can be observed by changing the frequency of the applied electric field. The crossover frequency, f_{x_0}, is defined as the frequency at which the force changes from positive to negative DEP. It is given as [25, 26, 27, 28]

$$f_{x_0} = \frac{1}{2\pi}\sqrt{-\frac{(\sigma_p - \sigma_m)(\sigma_p + 2\sigma_m)}{(\varepsilon_p - \varepsilon_m)(\varepsilon_p + 2\varepsilon_m}} \tag{5}$$

The value of f_{x_0} depends on the conductivity of the particle σ_p at low frequencies (<1 MHz) and on the permittivity of the particle ε_p at higher frequencies. The total conductivity, σ_p, of a spherical dielectric particle is given by the sum of its bulk, σ_{bulk}, and surface conductivity, K_s, [25, 26, 27, 28]

$$\sigma_p = \sigma_{bulk} + \frac{2K_s}{r} \quad (6)$$

The σ_p is mainly dependent on K_s because σ_{bulk} is negligible for very small particles. It should be noted that the polystyrene microspheres (PM) were used as dielectric particles in this experiment. The value of K_s varies significantly depending on the size and conjugation of the PM and acts as a way to isolate, concentrate, or separate different types of target bioparticles [26].

The other forces acting on the particle surrounded by the medium are drag force, electro-thermal force, buoyancy, and Brownian motion. So, the DEP force that depends on the electric field gradient should be strong enough to overcome these forces.

2.2. Drag Force

The drag force is due to motion that arises from the friction of the particle with the surrounding medium. For small spherical particles, such as polystyrene microspheres, the drag force due to the friction with surrounding fluids is given by:

$$F_{drag} = 6\pi\eta\nu r \quad (7)$$

where η is the viscosity of the medium, r is the radius of the particle, and ν is the velocity of the particle. Drag force works in the opposite direction of DEP force.

2.3. Electro-thermal Forces

To generate a strong DEP force, the design of the electrode is such that it can produce a high electric field. The electrodes are micro electrodes that have dimensions measured in μm. This high electric field generated in this small area produces a significant amount of heat to be dissipated to the surrounding fluid medium. The heat dissipation can be calculated by calculating the power dissipation of an electrode and its surrounding medium. For the surrounding medium, the power generated by the electric field, E, per unit volume of fluid is given as:

$$P_{medium} = \sigma E^2 \tag{8}$$

For the electrode, the heat as well as power generated by the applied voltage, V, is:

$$P = \frac{{V_{rms}}^2}{R} \tag{9}$$

Total power or heat dissipation is calculated by the summation of these two powers. The heat generated in a small area increases the surrounding temperature, and the increase in the temperature is given as:

$$\Delta T \approx \frac{\sigma {V_{rms}}^2}{k} \tag{10}$$

where σ and k are the electrical and thermal conductivity of the medium, respectively, and V_{rms} is the applied root mean square voltage.

As the DEP force is produced from the nonuniform electric field, the heat dissipation is also nonuniform. This nonuniform heating gives rise to further change of certain properties such as conductivity, viscosity, permittivity, and density of the medium. The temperature gradient created from the nonuniform heating and changes in these properties give rise to dielectric and electro thermal forces as well as buoyancy.

2.4. Buoyancy

Buoyancy is produced due to a nonuniform temperature change and the temperature gradient of the fluid that changes the density across the fluid and produces a natural convection. This force can be written as:

$$F_B = \frac{\partial \rho_m}{\partial T} \Delta T g \tag{11}$$

where ρ_m is the density of the medium, T is the temperature, and g is the acceleration due to gravity.

2.5. Brownian Motion

Particles experience Brownian motion in the fluid. Though the force from Brownian motion is negligible when compared with DEP force, the particles experience a little force due to this motion. The time average motion of the particles is zero. The motion experienced by a particle is given by:

$$F_{Brownian}(t) = m\frac{\partial v}{\partial t}6\pi\eta r v \tag{12}$$

where m is the mass of the particle, v is the velocity of the particle, and η is the viscosity of medium.

2.6. Negative DEP Biosensor

To design a negative DEP based biosensor with real time image processing and light scattering, an electrode chip was designed in Photonics lab [26, 27]. The electrode design was produced to generate strong DEP force with voltage 10 Vpp, and to create enough force that overcomes the other forces. Polystyrene microspheres (PM) were used as dielectric particle to observe the effect of DEP force and quantify the particles. A green LED with 45-degree angle was used to illuminate 720 nm PM, which scatter light through a Mie scattering process. A USB video class (UVC) standard compliance microscope camera was used to collect the images for real time image processing that can collect 25 frame per second. An application was built in the lab using Microsoft Visual C++ for the Windows operating system that collect the live videos through the camera and performed real time image processing [26]. From the time lapse images, the application calculated the drift velocity of the particles from their position and time during positive and negative DEP. The application produced the data for three color bands and for the green band, the spectrum of drift velocity vs frequency was plot. For various concentration

levels, the DEP spectrum was measured. The DEP spectrum can be used as an indication of the cancer stage of the patients.

3. ELECTRODE DESIGN AND SIMULATION

3.1. Design

A new electrode was designed for further reduction of the heat sources and to increase the electric field gradient on the tip of the electrode. Furthermore, the electrode was designed so one droplet of the sample fits on one electrode, and it can be reused. A 10-µL sample creates a droplet size of 6.44 × 4.65 mm with an average of 5.5 × 5.5 mm for design of the electrode layout. In this area, I wanted to fit $4 \times 4 = 16$ electrodes, whereas for the previous electrode, it was $25 \times 25 = 625$ electrodes. Therefore, the number of electrodes as well as heat sources were greatly reduced.

A depiction of the electrode design layout is presented in figure 5. From one tip to another tip of the electrode, the dimension was 1356 µm, which is one fourth of 5.5 mm (5.5 mm / 4 = 1356 µm; figure 5a). The radius of curvature of a tip was 20 µm, and the upper curvatures were 80 µm and 320 µm to ensure enough gap for the particles to remain only in a high electric field area (figure 5b).

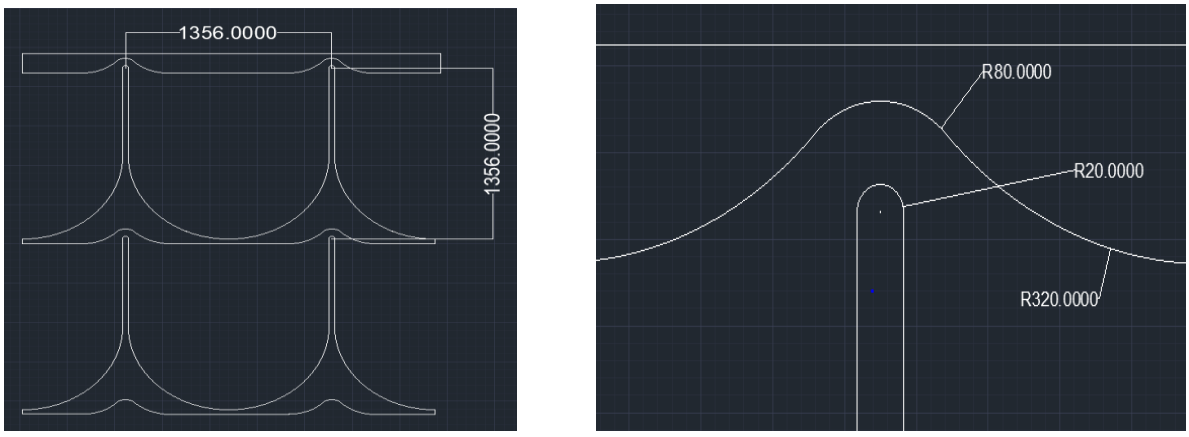

(a) (b)

Figure 5. Dimensions of the designed electrode in µm (a) 2x2 electrode (b) single tip of an electrode.

Two different electrode layout designs (figure 6a) were created so more electrodes could fit in a single 4-cm wafer (figure 6b). The electrode was fabricated on a commercially available glass wafer with standard fabrication procedures involving photolithography, metal sputtering, and lift-off procedures using 1000-Å thick gold film in the microfabrication facilities at North Dakota State University.

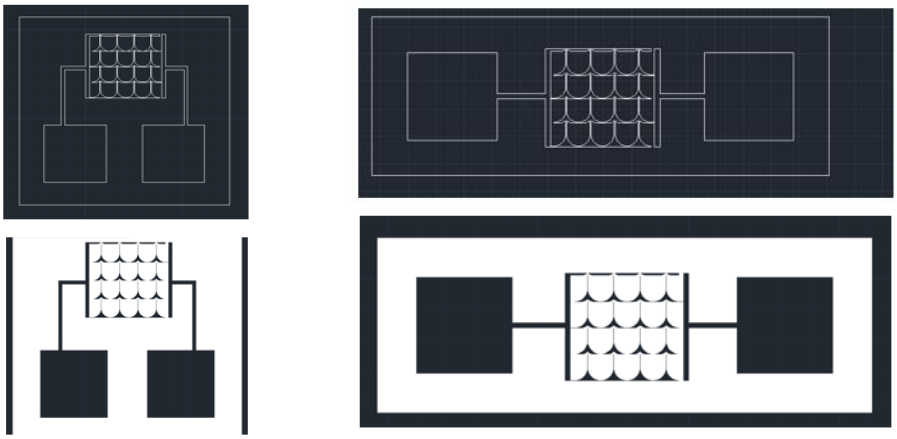

(a)

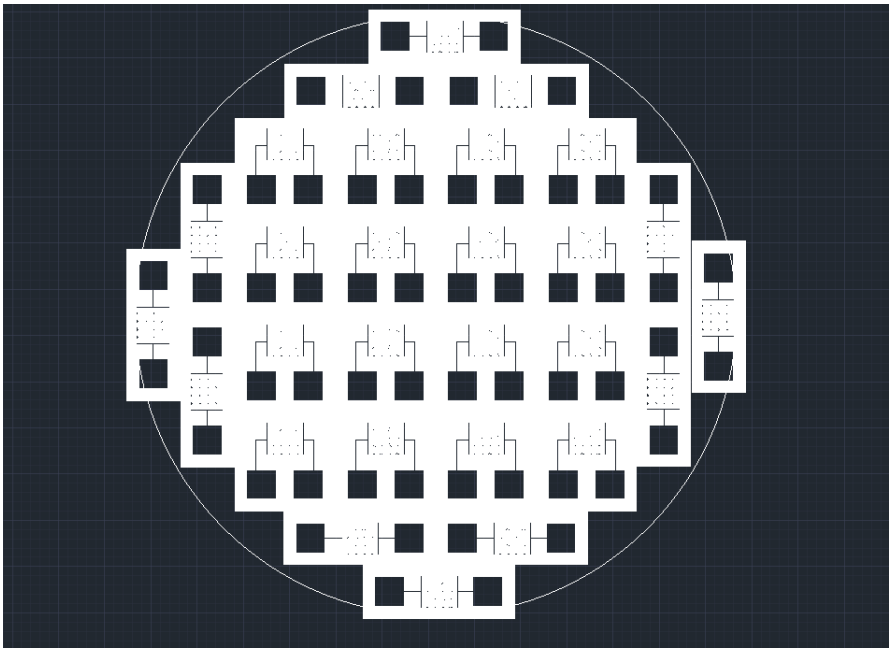

(b)

Figure 6. (a) Two different electrode designs with hatching (b) 4-cm wafer with hatching.

3.2. COMSOL Simulation

To measure the electric field gradient and electromagnetic heating in the tip of the electrode, simulations were performed using COMSOL Multiphysics 5.3a licensed version in NDSU Software facility. To create strong DEP effect on the tip of the electrode, the designed electrode should be able to produce high electric field gradient on the tip. Furthermore, the electric field gradient should be the highest only on the tip and gradually decrease toward the upper electrode. The simulation was performed to estimate the electric field gradient pattern and its maximum value. The electromagnetic heating is caused on the tip of the electrode due to the high electric field. This heating creates some problems such as fast drying of the conductive solution, which increases with the conductivity of the solution. So, the simulation was performed to monitor the temperature rise in certain periods of time. The steps and analysis of the simulations are explained below.

3.3. Electric Field Gradient Simulation

To measure the electric field gradient, a 3-D model of COMSOL was selected, and a layout with fewer electrodes was used to reduce the simulation time without distorting any measurements. At first, the AC/DC module was started, and then, the module of electric currents (ec) was selected. In the frequency dependent study, 120 kHz was used to observe the effect of the negative dielectrophoretic force. The electrode design was imported from the AutoCAD .dxf file, and the geometric length was chosen to be in μm. After importing the electrode design, a surrounding rectangular box was drawn to select the surrounding medium used in the simulation. For a liquid medium, a block was drawn above the rectangle after selecting the extrude extension with a thickness of 0.01 μm. From the material portal, different materials were selected such as gold as the element of the electrodes, glass as the blank parts of the electrodes, and water as the

element of surrounding medium. To run the simulation, the value for permeability and the conductivity of the liquid was adjusted to 83 and 0.005 S/m, respectively to represent PBS buffer. For the supply voltage, in the electric potential part of the simulation 10 V was selected for one electrode domain and 0 V for the adjacent electrode domain.

In the mesh, for faster simulation, various mesh size can be created. For a fixed electrode area, I drew a box and took a free triangular domain and selected a smaller size of the mesh for this domain that was 0.001 μm. For the remaining part of the electrode area, a larger mesh size of normal mesh was selected, and the mesh was built accordingly, as in figure 7.

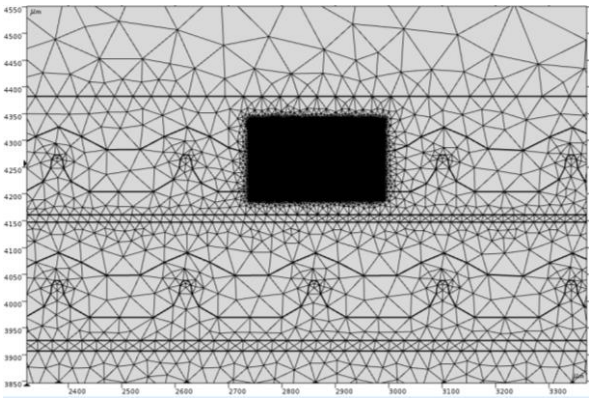

Figure 7. Various mesh sizes with lower mesh in black rectangular region.

After building the mesh, for the study portion of the simulation, the frequency 120 kHz was selected, and the total simulation was computed. The result of electric potential was produced as shown in figure 8. To calculate the electric field gradient, a surface was added to the electrical potential portal and the equation was set for electric field gradient with the following equation in the software:

$$G = \sqrt{\left(\frac{d(ec.normE^2)}{dx}\right)^2 + \left(\frac{d(ec.normE^2)}{dy}\right)^2} \quad (13)$$

Where *G* is the magnitude of electric field gradient and *ec.normE* is the magnitude of normalized electric field in V/m.

To observe the variation of the electric field, cut lines and edges were selected simultaneously, and in the plot section, the color map produced is demonstrated in figure 9. The electric field gradient was as high as 1×10^{16} V^2/m^3, which is needed to have a strong DEP effect to overcome other forces such as electrothermal force, Brownian motion, and drag force.

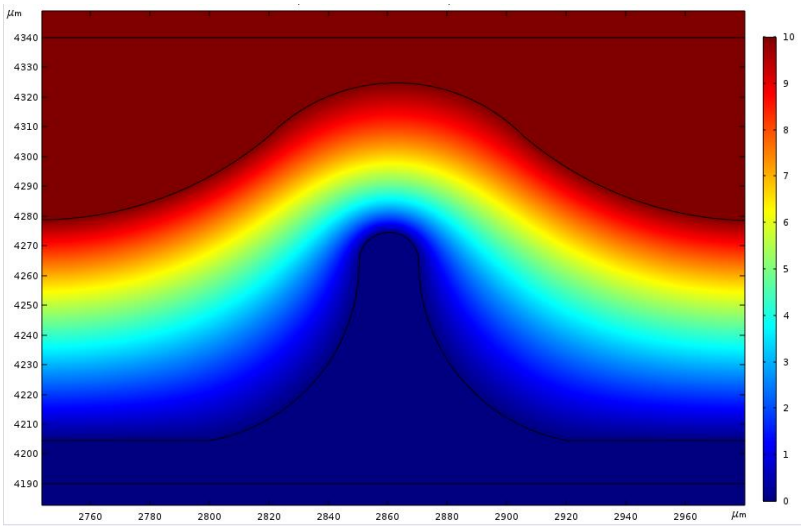

Figure 8. Electric potential (0 to 10 V) on the plane of the electrode.

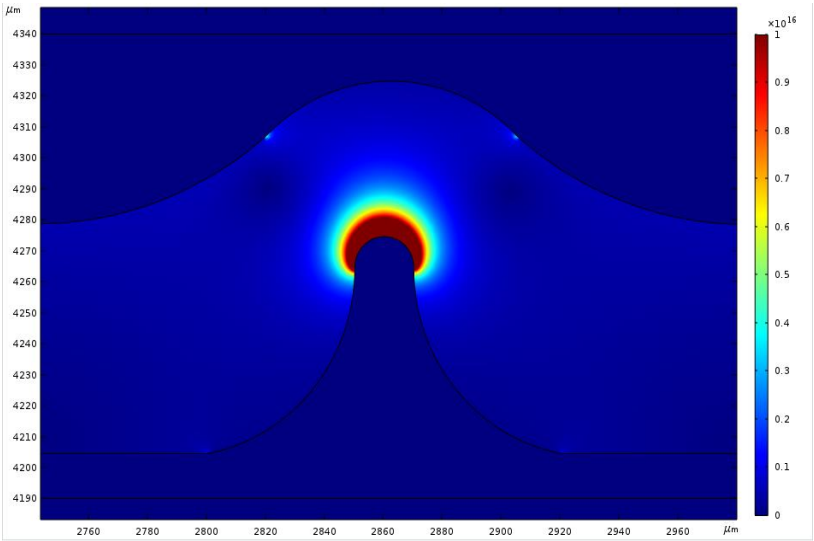

Figure 9. Electric field gradient (0 to 1×10^{16} V^2/m^3) on the plane of the electrode.

3.4. Electromagnetic Heating Simulation

Electromagnetic heating is produced in the tip of the electrode due to the high electric field gradient. In these locations, the electric field gradient was as high as 1×10^{16} V^2/m^3 according to our simulation and experiment. This high electric field gradient in this small area created heating, and this heat effect increased the conductivity of the 0.001x Phosphate Buffet Saline (PBS) above the baseline conductivity of 0.005 S/m. For the simulation or the Bovine Albumin Serum (BSA), this heat increases the conductivity of the solution above the baseline conductivity of 0.003 S/m. This heating caused faster drying of the fluid, PBS or BSA, due to evaporation and further concentrated the fluid with higher conductivity that also causes erosion of the tip of the electrode. The simulation was performed to measure the temperature rise at certain times (after 3 and after 18 minutes). The simulation procedure in COMSOL is described below:

At first, a 3-D model was selected to calculate heat with the surrounding flux and spread of the temperature in the ambient atmosphere. An electromagnetic heating portal was selected from the heat transfer module and the joule heating was chosen from the electromagnetic heating portal. To measure the temperature in terms of time, the time dependent study was created, and the geometry of the electrode was imported from the AutoCAD design. To create the surrounding material, a rectangular box was drawn similar to the electric field gradient simulation, and blocks were built above and beneath the rectangular box after extruding the electrode to a thickness of 0.01 μm. In the material portal, gold was selected for electrode, water with adjusted conductivity and permittivity for PBS was selected for fluid, and glass was selected for electrode blank space and lower block. The Electric Current Physics section in joule heating had an electric potential that was set to 10 Vpp, similar to the electric filed gradient

simulation. In the heat transfer module for the solid section, heat source, heat flux, and fluid were added as the portals. The boundaries were selected for the fluid and solid materials. The electrodes were the only heat sources, and the initial temperature of these sources was set to 300 K. The thermal insulation was avoided, and in the heat flux portal, convective heat flux was selected, and air flux was set to $20\ W/m^2K$.

To create the mesh and for faster 3-D simulation, sweep mesh was used by adding a free triangular portal and setting a smaller size for the electrode face that gradually increases in size to the blocks. The maximum size was 0.05 µm and minimum size was 0.01 µm. After building the mesh, in the study section, time was selected from 0 to 5 minutes with an increment of 0.1 minutes, and it was computed.

Figure 10 shows the temperature after 3 minutes and after 18 minutes. Any slice from any axis can be checked for the temperature change. The electrode slice was chosen such that on the top of the electrode surface, which is considered to be the mostly heated area. After 3 minutes applying a 10 Vpp difference of potential, the temperature was increased by 1 K. After 18 minutes, the temperature increased by 2 K, depicted in figure 10.

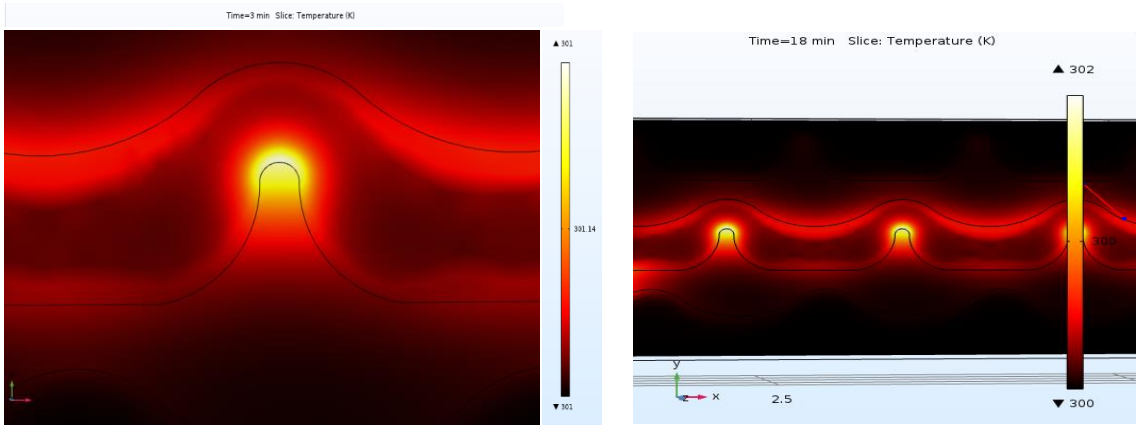

(a) (b)

Figure 10. Electromagnetic heating after (a) 3 minutes and (b) 18 minutes.

4. EXPERIMENTAL SETUP

4.1. Sample Preparation

Polystyrene microspheres (PM) were used as dielectric particles for the DEP force. Samples were prepared with antibody-antigen binding from protein biomarkers as in ref. [27]. The steps for sample preparation are demonstrated below.

4.1.1. Biotinylated PM Avidin Conjugation

According to the manufacturer's recommendation for 100% binding, 3 µL of Avidin must be mixed with 10 µl of biotinylated PM. Then the 13 µL of Avidin and PM were mixed with 387 µL of 0.001x PBS for a total of 400 µL and mixed using the vortex machine for about 5 seconds. To bind the Avidin and Biotin, the sample was put in a shaker for 20 minutes. Then the sample was put in a centrifuge machine at 14,000 rpm for 5 minutes in order to easily remove the buffer. After centrifuging, the Avidin conjugated Biotinylated PM was separated from the solution and buffer was removed using a pipet carefully to avoid the loosely connected bindings.

4.1.2. Biotinylated CA 242 Antibody Attachment to the Biotinylated PM + Streptavidin

According to the manufacturer's recommendation for 100% binding, 3 µL of Biotinylated CA 242 was mixed with 397 µL of 0.001x PBS containing 10 µL of biotinylated PM + Streptavidin for a total of 400 µL. The mixture was then put in a vortex machine for 5 seconds and then in a shaker for 20 minutes. The sample was then put in a centrifuge at 14,000 rpm for 5 minutes in order to easily remove the buffer. After centrifuging, the CA 242 antibody attached Avidin conjugated Biotinylated PM was separated from the solution and the buffer was carefully removed using a pipette.

4.1.3. Preparing the Sample for Various Concentrations of CA 242 Antigen

In serum there are various concentrations of cancer antigens. This research focused on the CA 242 antigen. Thus, we prepared a Bovine Albumin Serum (BSA) spiked with three concentrations of CA 242 antigen: 10, 20, 40 U/mL, and a control group without CA 242. The BSA was prepared with DI water in a concentration of 0.1 g/L. The serum was spiked with concentrations of CA 242 prepared according to the provided sample concentration of $15{,}000\times 10^3$ U/mL. The calculations for the sample preparations were as followed:

- The total volume of each sample was 400 µL.
- 0 U/mL was the only Avidin conjugated Biotinylated PM prepared sample without the CA 242 antigen.
- The $15{,}000\times 10^3$ U/mL sample was diluted in serum by $\frac{1}{1000}$ times so that it became 15,000 U/mL; the equation to calculate each concentration level is:

$$\frac{15000 \times x}{400} = desired\ concentration$$

- Therefore, for 10 U/mL, $x\sim 0.27$ µL; for 20 U/mL, $x\sim 0.53$ µL; and for 40 U/mL, $x\sim 1.07$ µL.

After the serum samples were prepared, they were then mixed with the prepared PM samples with CA 242 antibody, and the tubes were marked in order to identify them easily. The samples were vortexed and put in a shaker for 20 minutes. Then they were centrifuged at 14,000 rpm for 5 minutes. After centrifuging, the serum was removed and a 400 µL of 0.001x Phosphate Buffer Saline (PBS) was added to each tube. This centrifuging process was done three times for the complete removal of the serum. For each concentration level, 10 µL were taken and put on the electrode under the microscope in order to perform six replications of the experiment.

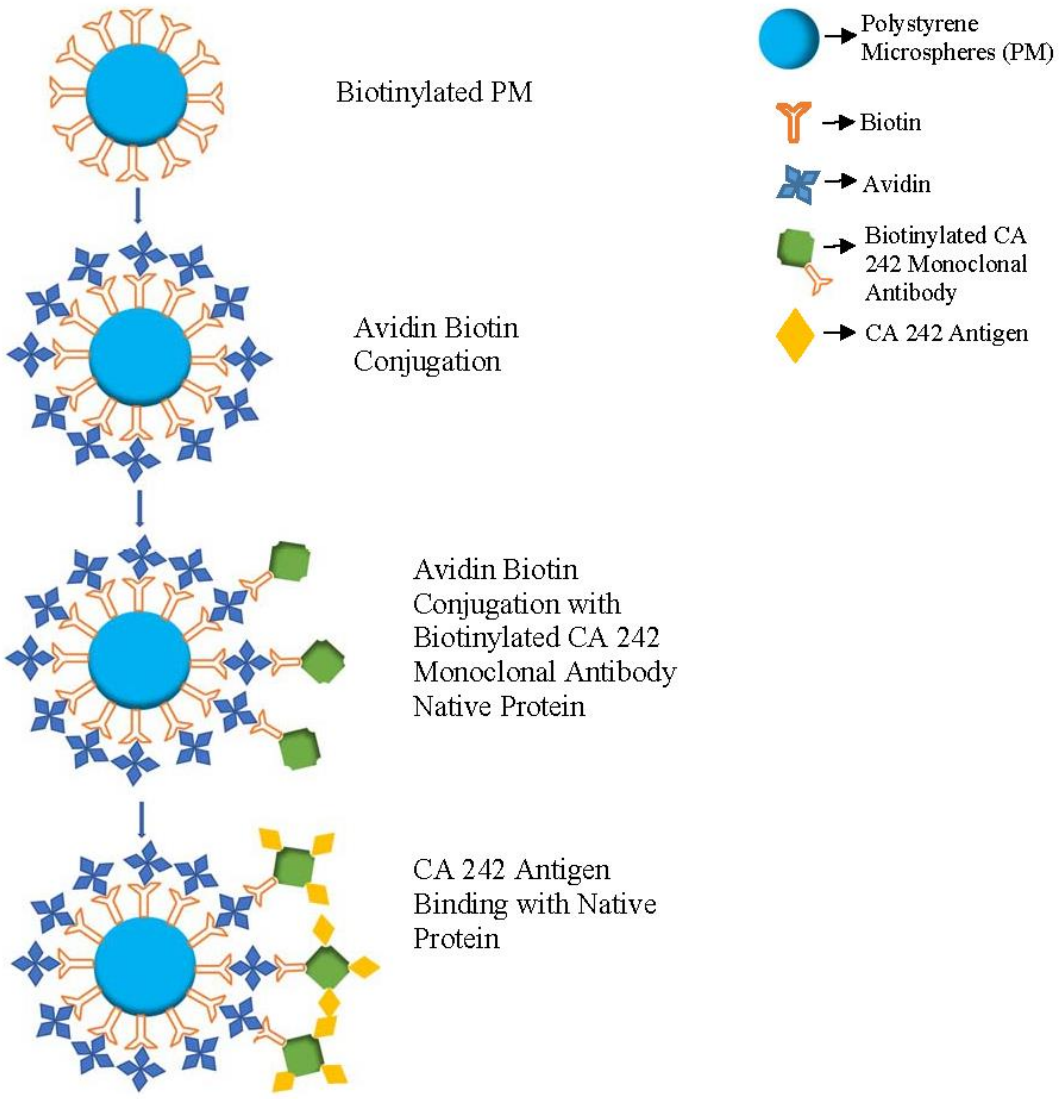

Figure 11. Sample preparation.

4.2. Setup Explanation

The experimental equipment with already prepared samples is shown in Figure 12. The main system consisted of a personal computer with a Windows operating system, an OMFL600 low power microscope, a UVC compliant ProScope PS-MC5UW microscope camera, an LED illumination, a fabricated electrode array chip, and a Tektronix AFG3021B function generator as in ref. [31, 32]. The microscope was placed on an optical tabletop (purchased from Newport

Corporation) to avoid any vibrational noise. For the image processing, the image processing software, which was built for the DEP spectroscopy in this lab, was installed and run on the computer.

The samples were prepared with Biotinylated polystyrene microspheres and the CA 242 antibody and the antigen. Then 10 µL of the sample were pipetted, put on the electrode, and placed under the camera connected with the microscope. The terminals of the electrode were connected to the function generator and it is placed in an electrode well plate which is designed for the specific electrode size. Then it was cleaned with alcohol and wiped to avoid any contamination. The adhesive tape was also used to firmly attach the electrode with the well-plate as it did not get distorted with any movement during the experiment. The green LED side illumination is placed at 45 degrees for the Mie scattering in the 720 nm bead samples. The camera fed the software with real-time images when the application is started. The application automatically controls the time as well as the frequency of the function generator. The voltage supplied is 10 V peak-to-peak and the frequency was swept from 500 kHz to 2,000 kHz with an increment of 300 kHz, which corresponds to six frequencies. At first, the positive DEP was applied with 10 kHz for 60 seconds to accumulate the beads to the tip of the electrode and the 40 milliseconds negative DEP was applied to repel them from the tip of the electrode. Depending on the DEP force the position, as well as the drift velocity, was changed, and those values were stored in the application process. With these values, the drift velocity vs. frequency spectra was generated.

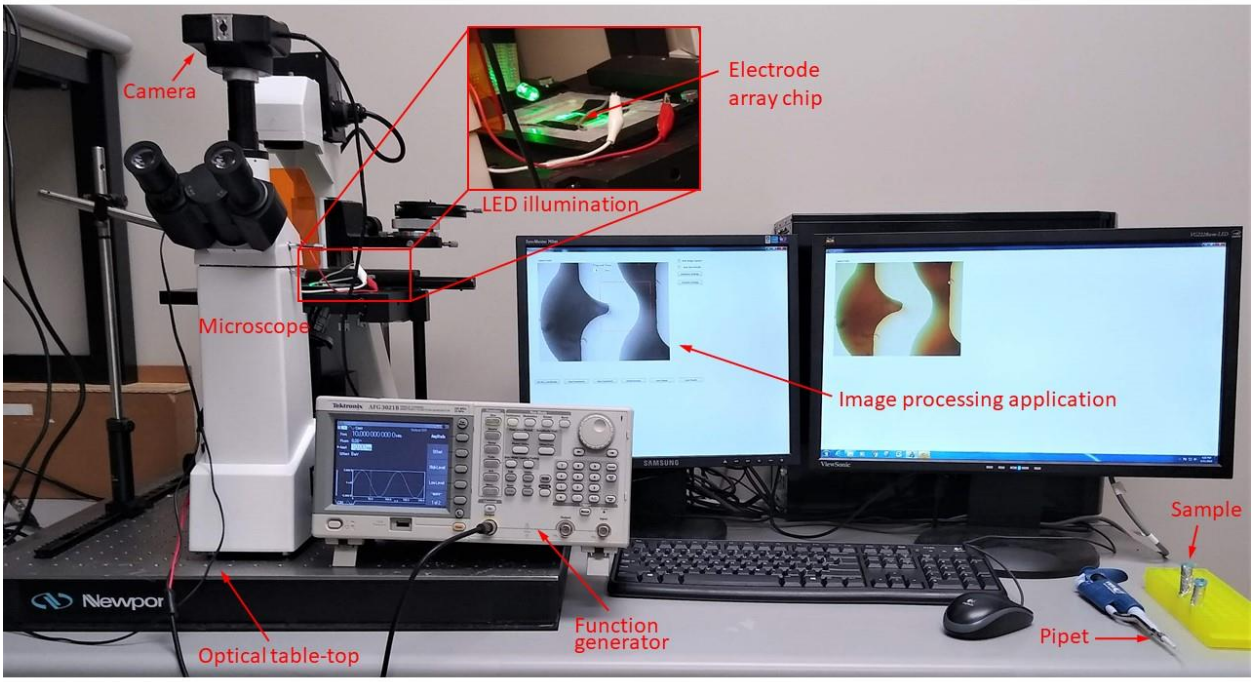

Figure 12. Experimental setup.

5. RESULT AND DISCUSSION

Using DEP spectroscopy application that uses real-time image processing, the spectrum of various levels of CA 242 was generated. The camera collected images of the electrode under a microscope as in figure 13, where the red scale bar indicates the 50 µm dimension. The box was defined as the region of interest for the ease of image processing. The image processing software was developed by Fleming D. Gudagunti [27] after improving the original version of that software developed by Syed A. M. Kirmani [26].

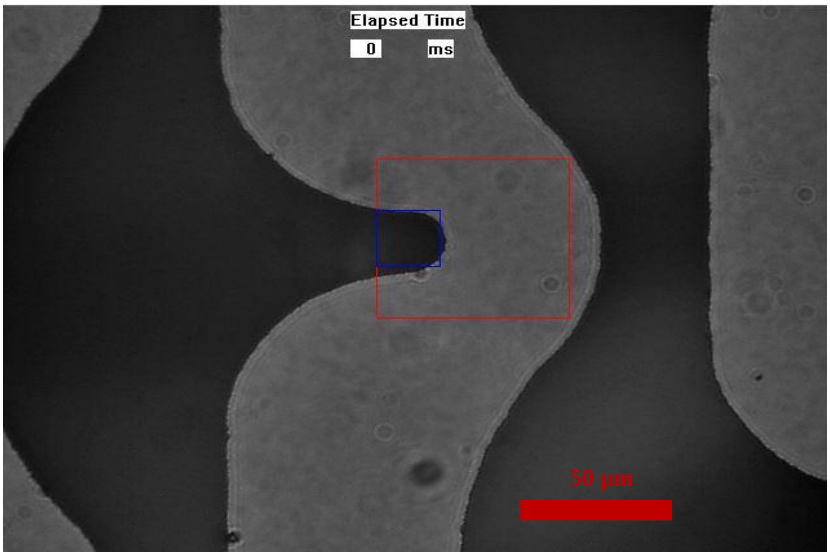

Figure 13. Electrode imaged by a microscope with a 25x objective.

From figure 14, the effect of the positive and negative DEP force can be observed. During positive DEP, particles are attracted to the higher electric field gradient area, which is in the tip of the electrode, and during negative DEP, particles are repelled from the tip of the electrode.

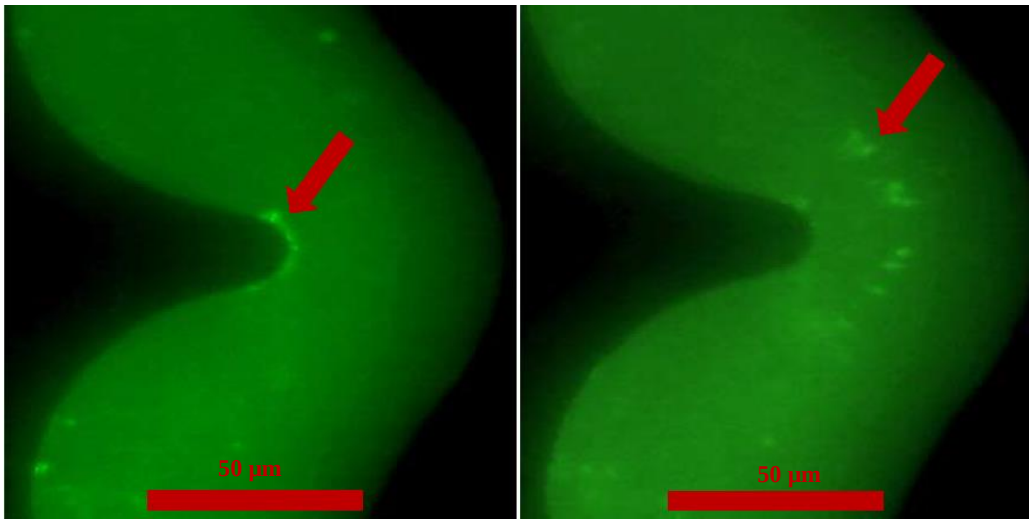

Figure 14. Positive and negative effect of DEP.

Experiments were performed six times for every concentration of CA 242, and the spectrum gives the error bars of those experimental values. (figure 15)

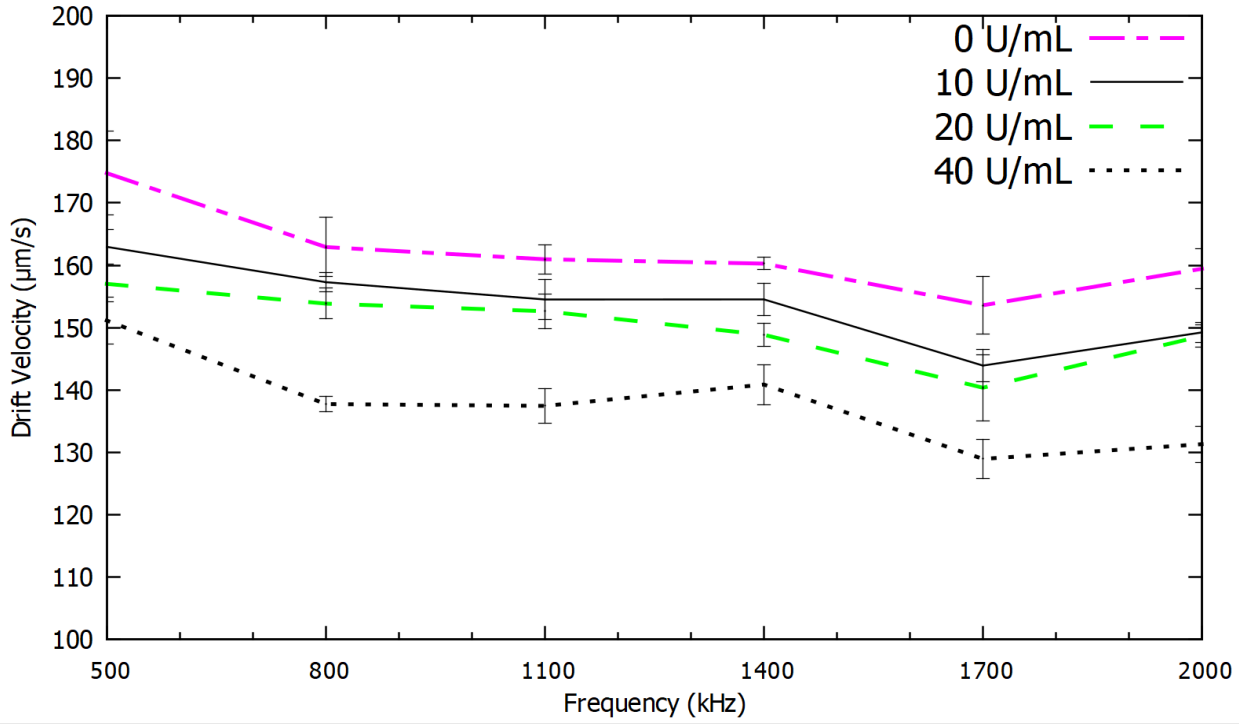

Figure 15. Negative DEP spectrum for the various concentration levels of CA 242.

From the spectrum, it can be clearly observed that there are clear distinctions among the spectra for various concentration levels for the frequency ranges from 500 kHz to 2,000 kHz.

The cut-off levels for CA 242 is 20 U/mL, and it represents the first stage of cancer. Here, lower than 20 U/mL were also measured which are 0 U/mL and 10 U/mL. Using these spectra, it is possible to determine the pancreatic cancer antigen CA 242 as well as cancer at the very early stage. Furthermore, using only one frequency and one concentration, the experiment time was less than 5 minutes for example for 1,700 kHz 40 U/mL concentration level. So, this method was faster than the existing methods to detect cancer in its first stage, and this method can be potentially used for the diagnosis and prognosis of pancreatic cancer.

6. CONCENTRATION PREDICTION MODEL

From the experiment, a DEP Spectrum was generated for various concentration levels of CA 242. Using this spectrum, a method was developed for automatically predicting a concentration value using these experimental values. The concentration of cancer biomarkers is unknown in a serum sample collected from a patient. This model identified this unknown concentration using the spectrum values for 0, 5, 10, 20, and 40 U/mL CA 242. At first, a non-linear third order polynomial regression was used for the prediction model shown in figure 16.

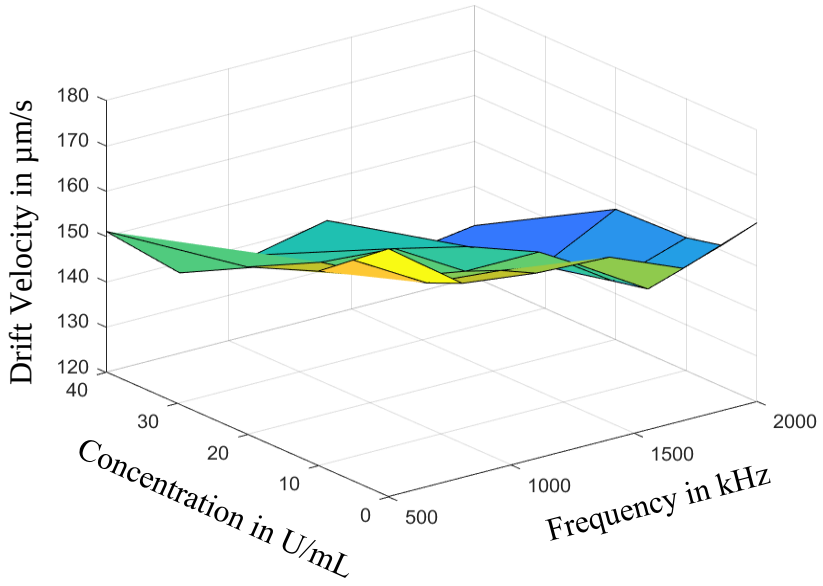

Figure 16. Predicted model with polynomial regression.

Using the four concentrations as training values, the 5th concentration was predicted. Below is a table (table 3) of predicted concentrations with percentage accuracy.

Table 3. Concentration prediction with polynomial regression.

Actual Concentration	Predicted Concentration	Relative Error
5 U/mL	6.7814 U/mL	-0.35628
10 U/mL	10.6705 U/mL	-0.06705
20 U/mL	17.9279 U/mL	0.103605

As, only six experiments were performed due to many constraints such as cost and time, using the means and standard deviations (SD) from those experiments, pseudo samples were produced to regenerate the data using Gaussian Distribution using the Bootstrap method. For each frequency and concentration, the drift velocity was created 1000 times. From the six experimental frequencies and five experimental concentrations, 30,000 values were generated. From those values, error histograms were generated for the prediction model, and a new predictive model was drawn with relative error values (figure 17).

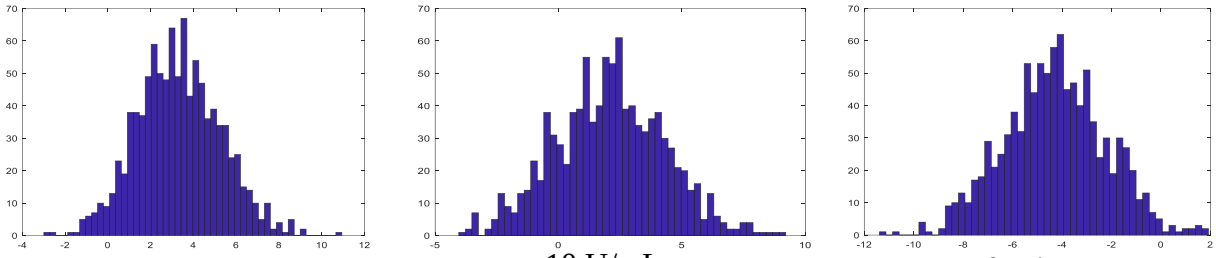

Figure 17. Error histogram for different concentration prediction obtained using the Bootstrap method (Relative error in x axis and number of samples in y axis).

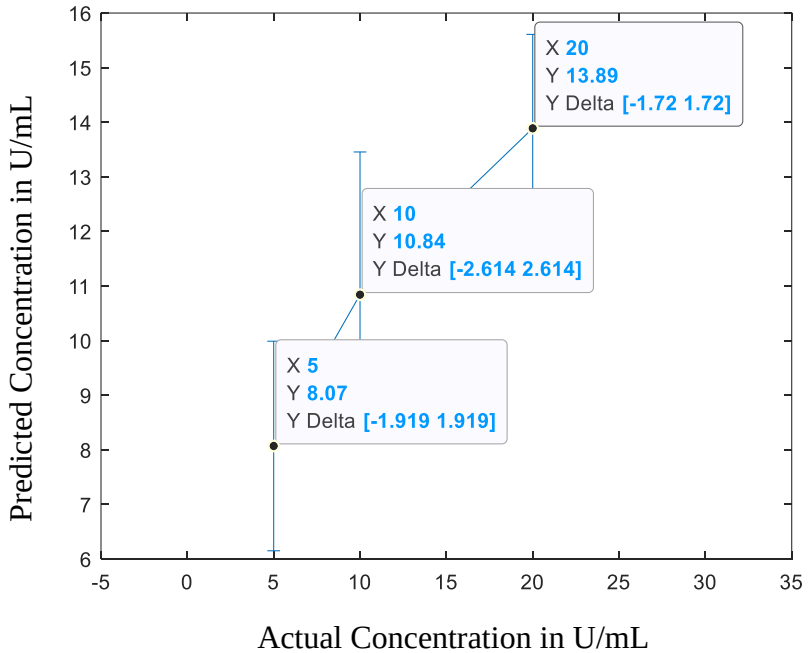

Figure 18. Predicted concentration and the confidence interval (SD) obtained using the Bootstrap method.

The flow chart for the process is given below.

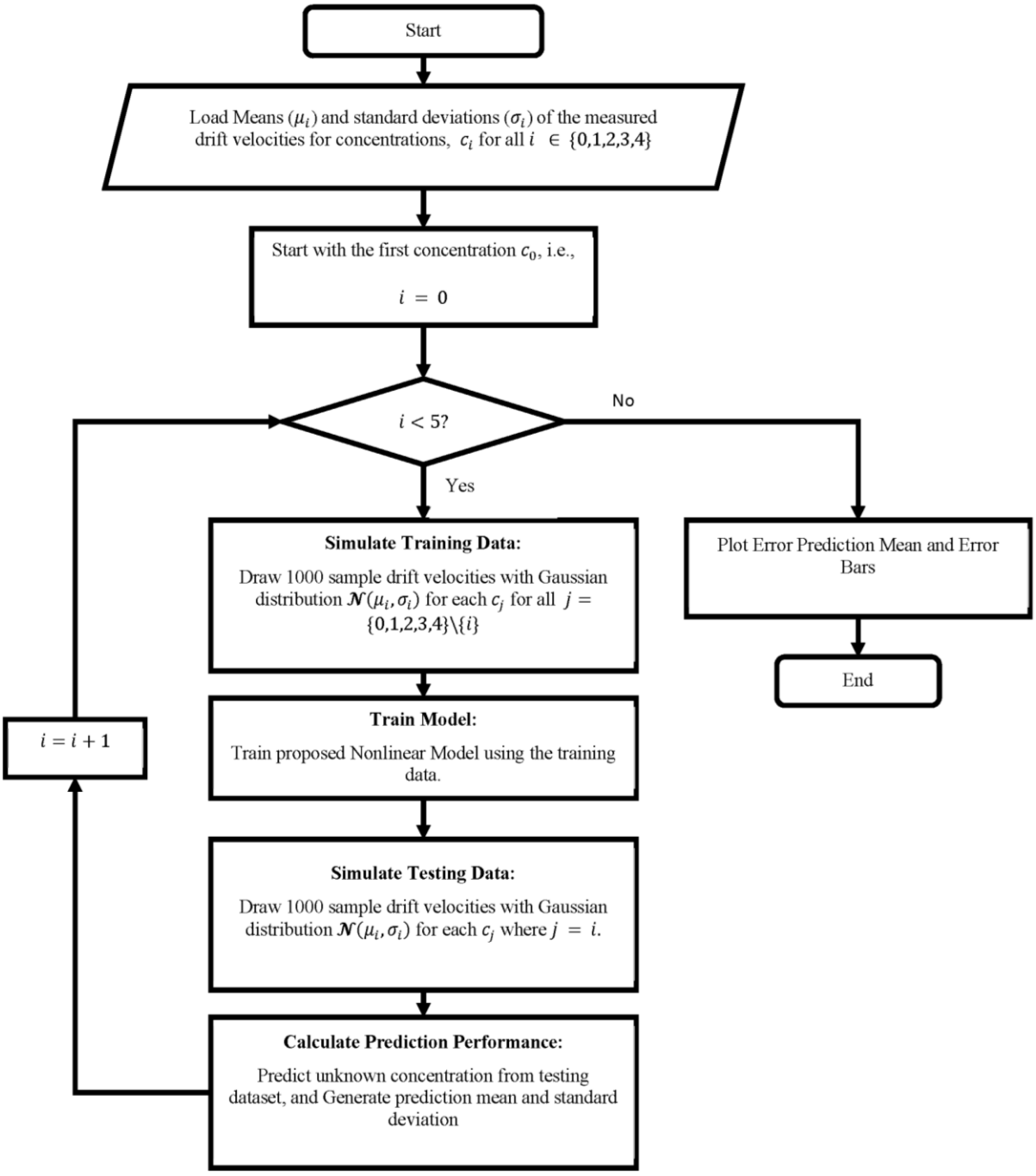

Figure 19. Flow chart of the concentration prediction algorithm using the Bootstrap method.

7. CONCLUSION

In this thesis, a method for detecting pancreatic cancer was demonstrated. This biosensor used negative DEP as an effective transduction mechanism with image processing and light scattering, that can be potentially used for the first stage cancer diagnosis. This method is cost effective and fast technique which can detect the cancer protein biomarker within shorter period of times. In this thesis, pancreatic cancer biomarker CA 242 was analyzed that has high sensitivity and specificity and serum sample was used rather than PBS buffer. BSA was used as serum in this experiment. Therefore, this method can be used in practiced to screen blood sample from patients for diagnosis. Furthermore, a simulation work was presented with the analysis of electric field gradient and electromagnetic heating in the tip of the electrode. A new design of electrode array chip was demonstrated with an improvement of temperature constraint that can be used in future experiments. A concentration prediction model was built to automatically predict the concentration level from serum samples using the generated spectra from the experiment. This model can be simultaneously used with the generated spectra for real-time concentration prediction from the serum sample of patient which concentration is unknown.

REFERENCES

1. Jin, Cheng, and Ling Bai. "Pancreatic Cancer–Current Situation and Challenges." Gastroenterol Hepatol Lett 2, no. 1 (2020): 1-3.
2. Ladd, Jon, Hailing Lu, Allen D. Taylor, Vivian Goodell, Mary L. Disis, and Shaoyi Jiang. "Direct detection of carcinoembryonic antigen autoantibodies in clinical human serum samples using a surface plasmon resonance sensor." Colloids and Surfaces B: Biointerfaces 70, no. 1 (2009): 1-6.
3. Gupta, Vishal, Insiya Jafferji, Miguel Garza, Vladislava O. Melnikova, David K. Hasegawa, Ronald Pethig, and Darren W. Davis. "ApoStream™, a new dielectrophoretic device for antibody independent isolation and recovery of viable cancer cells from blood." Biomicrofluidics 6, no. 2 (2012): 024133
4. Raimondi, Sara, Albert B. Lowenfels, Antonio M. Morselli-Labate, Patrick Maisonneuve, and Raffaele Pezzilli. "Pancreatic cancer in chronic pancreatitis; aetiology, incidence, and early detection." Best practice & research Clinical gastroenterology 24, no. 3 (2010): 349-358.
5. Hidalgo, Manuel. "Pancreatic cancer." New England Journal of Medicine 362, no. 17 (2010): 1605-1617.
6. Wolfgang, Christopher L., Joseph M. Herman, Daniel A. Laheru, Alison P. Klein, Michael A. Erdek, Elliot K. Fishman, and Ralph H. Hruban. "Recent progress in pancreatic cancer." CA: a cancer journal for clinicians 63, no. 5 (2013): 318-348.
7. Vogelstein, Bert, and Kenneth W. Kinzler. "Cancer genes and the pathways they control." Nature medicine 10, no. 8 (2004): 789-799.

8. Ingvarsson, Johan, Christer Wingren, Anders Carlsson, Peter Ellmark, Britta Wahren, Gunnel Engström, Ulrika Harmenberg, Morten Krogh, Carsten Peterson, and Carl AK Borrebaeck. "Detection of pancreatic cancer using antibody microarray-based serum protein profiling." Proteomics 8, no. 11 (2008): 2211-2219.

9. Hussain, S. Perwez. "Pancreatic cancer: current progress and future challenges." International journal of biological sciences 12, no. 3 (2016): 270.

10. Singhi, Aatur D., Eugene J. Koay, Suresh T. Chari, and Anirban Maitra. "Early detection of pancreatic cancer: opportunities and challenges." Gastroenterology 156, no. 7 (2019): 2024-2040.

11. Choe, Jung Wan, Hyo Jung Kim, Jae Seon Kim, Jaehyung Cha, Moon Kyung Joo, Beom Jae Lee, Jong-Jae Park, and Young-Tae Bak. "Usefulness of CA 19–9 for pancreatic cancer screening in patients with new-onset diabetes." Hepatobiliary & Pancreatic Diseases International 17, no. 3 (2018): 263-268.

12. Ni, X. G., X. F. Bai, Y. L. Mao, Y. F. Shao, J. X. Wu, Y. Shan, C. F. Wang et al. "The clinical value of serum CEA, CA19-9, and CA242 in the diagnosis and prognosis of pancreatic cancer." European Journal of Surgical Oncology (EJSO) 31, no. 2 (2005): 164-169.

13. Ozkan, Hasan, Muhsin Kaya, and Abdulkadir Cengiz. "Comparison of tumor marker CA 242 with CA 19-9 and carcinoembryonic antigen (CEA) in pancreatic cancer." Hepato-gastroenterology 50, no. 53 (2003): 1669-1674.

14. Haglund, Caj, Johan Lundin, Pentti Kuusela, and Peter J. Roberts. "CA 242, a new tumour marker for pancreatic cancer: a comparison with CA 19-9, CA 50 and CEA." British journal of cancer 70, no. 3 (1994): 487-492.

15. Lundin, Johan, Peter J. Roberts, Pentti Kuusela, and Caj Haglund. "Prognostic significance of serum CA 242 in pancreatic cancer. A comparison with CA 19-9." Anticancer research 15, no. 5B (1995): 2181-2186.

16. Zhang, Yimin, Jun Yang, Hongjuan Li, Yihua Wu, Honghe Zhang, and Wenhu Chen. "Tumor markers CA19-9, CA242 and CEA in the diagnosis of pancreatic cancer: a meta-analysis." International journal of clinical and experimental medicine 8, no. 7 (2015): 11683.

17. Islam, Muhammad Torequl, and Mohammad Ashab Uddin. "Biosensors, the emerging tools in the identification and detection of cancer markers." Journal of Gynecology and Women's Health 5, no. 4 (2017): 555667.

18. Qian, Lisheng, Qiaobin Li, Kwaku Baryeh, Wanwei Qiu, Kun Li, Jing Zhang, Qingcai Yu et al. "Biosensors for early diagnosis of pancreatic cancer: a review." Translational Research 213 (2019): 67-89.

19. Ladd, Jon, Hailing Lu, Allen D. Taylor, Vivian Goodell, Mary L. Disis, and Shaoyi Jiang. "Direct detection of carcinoembryonic antigen autoantibodies in clinical human serum samples using a surface plasmon resonance sensor." Colloids and Surfaces B: Biointerfaces 70, no. 1 (2009): 1-6.

20. Luo, Xiliang, and Jason J. Davis. "Electrical biosensors and the label free detection of protein disease biomarkers." Chemical Society Reviews 42, no. 13 (2013): 5944-5962.

21. Zangar, Richard C., Don S. Daly, and Amanda M. White. "ELISA microarray technology as a high-throughput system for cancer biomarker validation." Expert review of proteomics 3, no. 1 (2006): 37-44.

22. Gudagunti, Fleming Dackson, Vidura Jayasooriya, Sharmin Afrose, Dharmakeerthi Nawarathna, and Ivan T. Lima. " Quantification of Pancreatic Cancer Antigen CA 242 using Dielectrophoresis." BMES, (2019).

23. Pohl, Herbert A. "The motion and precipitation of suspensoids in divergent electric fields." Journal of Applied Physics 22, no. 7 (1951): 869-871.

24. Pohl, Herbert A. Dielectrophoresis: The behavior of neutral matter in nonuniform electric fields (Cambridge Monographs on physics). Cambridge/New York: Cambridge University Press, 1978.

25. R. Pethig, “Dielectrophoresis: Status of the theory, technology, and applications,” Biomicrofluidics 4(2), 22811, American Institute of Physics (2010) [doi:10.1063/1.3456626].

26. Kirmani, Syed AM, Fleming Dackson Gudagunti, Logeeshan Velmanickam, Dharmakeerthi Nawarathna, and Ivan T. Lima. "Negative dielectrophoresis spectroscopy for rare analyte quantification in biological samples." Journal of biomedical optics 22, no. 3 (2017): 037006.

27. Dackson Gudagunti, Fleming, Logeeshan Velmanickam, Dharmakeerthi Nawarathna, and Ivan T. Lima. "Label-free biosensing method for the detection of a pancreatic cancer biomarker based on dielectrophoresis spectroscopy." Chemosensors 6, no. 3 (2018): 33.

28. Velmanickam, Logeeshan, Darrin Laudenbach, and Dharmakeerthi Nawarathna. "Dielectrophoretic label-free immunoassay for rare-analyte quantification in biological samples." *Physical Review E* 94, no. 4 (2016): 042408.

29. Huang, Y., and R. Pethig. "Electrode design for negative dielectrophoresis." Measurement Science and Technology 2, no. 12 (1991): 1142.

30. Lapizco-Encinas, Blanca H., and Marco Rito-Palomares. "Dielectrophoresis for the manipulation of nanobioparticles." Electrophoresis 28, no. 24 (2007): 4521-4538.

31. Gudagunti, Fleming Dackson, Logeeshan Velmanickam, Dharmakeerthi Nawarathna, and Ivan T. Lima. "Biosensor for Pancreatic Cancer Biomarker Based on Dielectrophoresis and Image Processing." In 2018 IEEE Research and Applications of Photonics In Defense Conference (RAPID), pp. 1-2. IEEE, 2018.

32. Gudagunti, Fleming Dackson, Vidura Jayasooriya, Sharmin Afrose, Dharmakeerthi Nawarathna, and Ivan T. Lima. "Biosensor for the Characterization of Gene Expression in Cells." Chemosensors 7, no. 4 (2019): 60.